On the analysjs of collective motions of atoms in mineral structures, and the mechanism of the α-β polymorphic transition in quartz

On the analysis of collective motions of atoms in mineral structures, and the mechanism of the α-β polymorphic transition in quartz

Kuniaki KIHARA

Department of Earth Sciences, Kanazawa University. Kanazawa 920-1192

Abstract : Computer programs were prepared for analyzing the atom trajectories generated in molecular dynamics simulation (MDS), and applied to reinterpret the mechanism of the α-β polymorphic transition in quartz (SiO_2). The programs contain the parts for calculating atomic quantities such as bond distances, angles and mean square displacements, and for collective ones such as X-ray scattering intensities, power spectral densities and normal modes. With the aid of a simplified structure model composed of atom sites of double-minimum potentials, the atomic mechanism of the α-β transition in quartz generated in the simulations was successfully interpreted. A transfer mode, in which atoms can move over the energy barriers between the double-minimum wells, is excited as an extra mode with an optic character even in the low-temperature phase (α), and the α-β transition is driven by the softening of this mode. The strong softening of this mode near the transition point also causes, via mode coupling, the softening of the two transversal acoustic branches with low frequencies in some ranges of small wave vector **q** in Γ-M, which cause the characteristic diffuse scattering and may cause the incommensurate satellite reflections observed when temperature approaches to the transition point.

1. Introduction

Since the discovery of X-ray diffraction by Max von Laue, structural analyses have been performed for a large number of minerals. So far, structural data (lattice constants, atomic coordinates, atomic temperature factors and so on) and their temperature or pressure dependencies have been available with enough accuracy. Now it is important to ask ourselves whether or not we sufficiently understand the true mechanism of phenomena in minerals. Atomic coordinates, displacement parameters and so on obtained in usual diffraction analyses are time and space averages in principle, where the details of atom dynamics are lost in the averaging processes. For example, the strange thermal-expansion in quartz is obviously caused by the collective behaviors of atoms. The knowledge of atom dynamics is crucially important in discussing every property of this and many minerals.

In molecular dynamics simulation (MDS) of solid structure, we can obtain atomic trajectories around the equilibrium positions in hypothetical structure characterized with given interaction parameters for atoms. Our crystals in MDS are of small atomic ensembles, much smaller than the practical crystals; in this sense, we may distinguish the crystals in MDS from the real ones referring to "MDS crystal". However, MDS has been applied to a large number of solid structures, and succeeded to produce the trajectory data of atoms,

whose averages are in good agreement with the atomic positions experimentally determined. Our stance is basically on reproducing reasonable structural data such as atomic positions, mean square displacements, spectroscopic data and so on in MDS, which must be comparable with those obtained in usual measurements. With the success of MDS in obtaining reasonable structural data, we infer dynamics in real crystals from analyzing the atom trajectories generated in MDS. Our purposes in this article are firstly to prepare computer programs to analyze the trajectory data in MDS crystal, and secondly to apply those to MDS quartz. As stated later, our MDS quartz was in harmony with the real crystal of quartz in most structural data. This article contains nine sections: sections 2 to 5 describe how the data are prepared for the comparison with experimental data. Sections from 6 explain those data obtained from MDS quartz, and the α-β transition mechanism and the dynamical aspect of internal structure at high temperatures are discussed. Computer programs developed in the present study are listed with brief explanations in section 8. Any detail about MDS calculations is not explained here.

2. Calculation of structural data
2.1. Lattice constants and atomic coordinates
In usual crystal analyses with diffraction data, lattice constants and point group are preliminary determined before intensity measurements. Symmetrically independent atomic parameters are determined with least-squares method applied to structure factors or their squares obtained from such diffraction intensities. The quantities obtained are time and space averages. To compare with the structural data, such as atom coordinates, atom mean square displacements (MSD) and so on, obtained in experiments, the time-dependent quantities in the MDS crystal must be averaged over time or space. (We must be careful whether or not the related processes are stationary.) The following analyses are all done without assuming any point group symmetry, but assuming constant translational symmetry. It may be possible to examine the point group and space group symmetries in the MDS crystal in that way.

In MDS for constant pressure, the size of crystal containing N basic cells, each of which contains n atoms, are given at every step of run. (The word "basic cell" is used here to represent the cell, whose multiple along their three edges is the MDS crystal.) The sizes of MDS crystal is represented with vectors $\mathbf{A}$, $\mathbf{B}$ and $\mathbf{C}$, whose components in Cartesian coordinates are arranged vertically to form a matrix of (3×3) lines and rows, which we call as $\mathbf{M}$ matrix. Lattice constants of Bravais lattice are calculated from $\langle\mathbf{M}\rangle$, the time average of matrix $\mathbf{M}$. Time-averaged $\langle\mathbf{r}_{\kappa\ell}\rangle$ is used to calculate space and time-averaged atomic positions as

$$\mathbf{r}_\kappa = \frac{1}{N}\sum_\ell^N \langle\mathbf{r}_{\kappa\ell}\rangle \qquad (\kappa = 1 \sim n),$$

which is ready to calculate fractional coordinates in the crystallographic unit-cell.

2.2. Atomic mean square displacements and probability density functions

The matrix of MSD of atom $\kappa(= 1\sim n)$ in a basic cell is calculated as time-average as

$$\mathbf{B}(\kappa) = \frac{1}{N} \sum_{\ell} < \mathbf{u}_{\kappa\ell} \mathbf{u}_{\kappa\ell}^{T} > , \qquad (2.1)$$

where super-script T means the transposed matrix, and

$$\mathbf{u}_{\kappa\ell} = \mathbf{r}_{\kappa\ell} - <\mathbf{r}_{\kappa\ell}>. \qquad (2.2)$$

This gives the time average of atom κ in the basic cell. Matrix **B** is diagonallized to provide MSD, $<u_{ii}^{2}(\kappa)>$, of thermal ellipsoid of atom κ, which is ready to be compared to quantities directly obtained from anisotropic atomic temperature factors β_{ij} in structure analysis. The probability density function (pdf) of atom κ is calculated by accumulating $\mathbf{u}_{\kappa\ell}$ over all atoms κ in the MDS crystal. The pdf obtained in this way may correspond to that obtained in a generalized structure analysis with structure factors developed in power series to higher order terms.

2.3. Atomic distances and angles

Atomic distances and angles resulted from usual structure analysis are $|<\mathbf{r}_i> - <\mathbf{r}_j>|$ and $<\mathbf{r}_i>$ - $<\mathbf{r}_j>$ - $<\mathbf{r}_k>$, respectively. It is further possible to calculate the averages of time dependent atomic distances and angles, i.e., $|<\mathbf{r}_i - \mathbf{r}_j>|$ and $<\mathbf{r}_i - \mathbf{r}_j - \mathbf{r}_k>$ with MDS results. In general, these two kinds of distances or angles are not identical, depending on the symmetries of related atomic sites; i.e.,

$$|<\mathbf{r}_i - \mathbf{r}_j>| \neq |<\mathbf{r}_i> - <\mathbf{r}_j>| \text{ or}$$
$$<\mathbf{r}_i - \mathbf{r}_j - \mathbf{r}_k> \neq <\mathbf{r}_i> - <\mathbf{r}_j> - <\mathbf{r}_k>.$$

The right side terms represent the distances and angles for averaged atomic positions, and not necessarily represent real distances and angles of bonds, respectively. The left side terms give the averages of distances or angles, and therefore provide the time-averaged values of true bond distances and angles in principle. In our X-ray structure analyses of quartz (Kihara, 2001 a), the Si-O distance (i.e., $|<r_{Si}>-<r_O>|$) shows decreasing tendency with increasing temperature. In our MDS quartz, we obtain the two kinds of values, $|<r_{Si}> - <r_O>|$ showing a similar tendency to the X-ray analysis and $|<r_{Si} - r_O>|$ showing a rather positive temperature dependence. These results led us to conclude that the real bond distance for Si-O expands with increasing temperature.

2.4. Order parameter and time-dependent displacement parameter of atom

A number of structural transitions from higher temperature phases to lower ones appear to

be driven by atomic departures from the positions of high symmetry to of low symmetry. In such a case, a thermodynamic function may behave as a function of such displacement or quantity termed as "order parameter" in general. Among a variety of possibilities, we employ the magnitude of departure of structure from that of high symmetry phase as order parameter. The temperature dependence of order parameter may depend on the nature and mechanism of the phase transition. We define a time-dependent "atomic displacement parameter" for MDS crystal. The temperature dependence of vibrational mode, which drives phase transition, could be identified to the power spectral densities generated for the time-dependent displacement parameters at atom sites. We define below the order parameter and displacement parameter for the case where atomic sites are characterized with double minimum potentials.

2.4.1. Model structure with atom-sites of double minimum potentials

Let a crystal has two kinds of atoms A (circles) and B (squares) in its orthogonal primitive unit-cell as shown in Fig. 1. The mean potential at each site has double minima, say α_1 (solid circles and squares) and α_2 (open circles and squares), separated by the energy barrier at the middle of minima, which may be denoted as "β-position" (open dotted circles and squares). This model may ease explaining atomic behaviors in the structure with atom-sites of double-minimum potentials. We below explain the structural behaviors expected or assumed for this model structure. The structure is assumed such that the relative arrangement of atoms is nearly kept in both the low (α) and high temperature (β) phases.

At lower temperatures of the low temperature phase, all the atoms vibrate in one of the double wells, α_1 (or α_2), i.e., the crystal is perfectly ordered, and one of the three optic
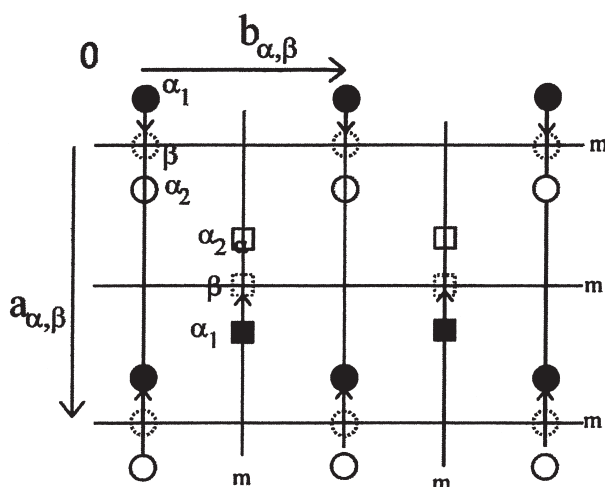
Fig. 1. A model structure of double-minimum potential energies.
    Circles represent atom A and squares atom B. At each atom site, energy minimum α_1 is indicated with solid circle (atom A) or solid square (atom B), and α_2 is open circle (atom A) or open square (atom B).

modes at Γ-point (wave vector **q**=0) is represented with the displacement pattern shown with arrows in Fig. 1. This mode drives all the atoms to move toward the β-positions between α_1 and α_2, and, therefore, could be the soft mode (SM) of the transition. However, the situation is not so simple as in the case, where atomic sites are of single-minimum potentials. With increasing temperature, the kinetic energies of atoms increase: in the present case, some atoms may be energized to go beyond the barrier to another well, α_2 (or α_1). At low temperatures, this kind of motions occurs separately in the crystal, and the atoms transferred may be restored to the original sides. In this way, a "transfer mode" is activated as an extra mode (to the normal modes). The point is that the transfer mode with larger amplitude has the same symmetry as the normal mode with smaller amplitude, in which atoms are confined either in the α_1 or α_2 wells. That is, the latter (normal) mode is not the true soft mode, but only boosts the transfer mode via coupling between them; in this sense, this mode is called QSM (quasi soft mode) hereafter. With increasing temperature, more atoms can transfer from α_1 to α_2, and the restoring force from α_2 to α_1 increases, depending on the ratio between the numbers of atoms staying in respective wells. Approaching to the transition temperature, the total driving force of the transfer mode, i.e., the difference between the restoring forces from both the sides decreases toward zero. That is, the frequency of the transfer mode decreases with temperature approaching to the transition point. When both the wells α_1 and α_2 are equally occupied by atoms, the positions averaged over their displacements become equal to those of the middle positions of α_1 and α_2, i.e., the high symmetry β-positions on the symmetry planes generated normal to the **a**-axis. The β-phase is thus resulted from the freezing out of the transfer mode, and in this sense, this mode is called as TSM (true soft mode) hereafter. In the higher symmetry β-phase, all the atoms are to be enough energized to move almost freely over the barriers, giving rise to a new normal mode with greater amplitude over the α_1 and α_2 wells, instead of QSM, which disappears or fades.

2.4.2. Atomic displacement parameter and order parameter

In the case of the model structure characterized with double-minimum potentials, we may represent the displacements (u_1, u_2, u_3) of atoms from their corresponding β-positions, such as

$$u_{1A} = - (x_A - 1/4)a_0, \ u_{2A} = u_{3A} = 0 \text{ and}$$
$$u_{1B} = (x_B - 3/4)a_0, \ u_{2B} = u_{3B} = 0, \tag{2.3}$$

where a_0 is the time-averaged **a**-axis dimension. A displacement may be normalized to dimensionless displacements (termed here "atomic displacement parameter") with the separations Δ_{AA} and Δ_{BB} for α_1-α_2 at sites A and B, respectively,

$$\delta_{1A} = 2u_{1A}/\Delta_{AA}, \quad \delta_{1B} = 2u_{1B}/\Delta_{BB}. \tag{2.4}$$

The normalizing process is necessary to relate the displacements to the macroscopic order parameter. Equation (2.4) represents vibrations confined in the potential wells in QSM at low temperatures, but even the transfer motions over α_1 and α_2 in TSM at high temperatures. It may be noted that the displacements contain two components of vibrational modes, QSM and TSM. The behaviors as represented with equation (2.3) are observed only in QSM and TSM, and therefore the components of atomic displacements parallel with the α_1-α_2 lines (the **a**-axis in this case) must be strongly contributed by QSM or TSM (δ_{1A} and δ_{1B}). The spectral densities of the space Fourier components of δ_{1A} and δ_{1B} at wave vector $\mathbf{q} = 0$ are to exaggerate the effects of QSM or TSM.

The normalized displacement parameters δ_{1A} and δ_{1B} can be generalized as $\delta_{j\kappa}$ for the directions j and atoms κ. Time-average $<\delta_{j\kappa}>$ is directly calculated for each of $Z = nN$ atoms, and then its average over all Z atoms is calculated in

$$\eta_j = \frac{1}{Z}\sum_{\kappa}^{Z} <\delta_{j\kappa}> \qquad (j = 1, 2, 3) \tag{2.5}$$

to represent the total order parameter of the crystal. A parameter is also defined in

$$\eta_{j\kappa} = \frac{1}{N}\sum_{p=1}^{N} <\delta_{p,j\kappa}> \quad (\kappa = 1 \sim n) \tag{2.6}$$

to represent displacements for each of n atoms in a basic cell, where $\delta_{p,j\kappa}$ represents the displacement of atom κ in the p-th basic cell. Both η_j and $\eta_{j\kappa}$ are the macroscopic order parameters, ready to compare with observed quantities in structure analyses.

η_j and $\eta_{j\kappa}$ are expected to be zero in the cases of $j = 2$ and 3, even in the double-minimum cases as suggested in Fig. 1. In the β-phase, η_1 is null, but shows strong temperature dependence in the α-phase, because of strong asymmetry of the transferring mode. That is to say, it is possible to represent the structural change in the crystal taking the unique parameter η_1, the order parameter. In general, the lines joining two minima are in different orientations from atom to atom, but a similar treatment to this case may be applicable, if appropriate internal coordinate systems can be chosen for all the atom sites. The α-β transition in quartz is this case.

3. X-ray scattering intensities
3.1. Total scattering intensities
The scattering amplitude of X-rays by an MDS crystal at time t is directly calculated as

$$Y(\mathbf{Q},t) = \sum_{\kappa=1}^{nN} f_\kappa(\mathbf{Q})e^{i\mathbf{Q}\cdot\mathbf{r}_\kappa(t)} , \tag{3.1}$$

where $f_\kappa(\mathbf{Q})$ is the scattering factor of atom κ, $\mathbf{r}_\kappa(t)$ atom position at time t, $\mathbf{Q}$ scattering vector ($Q = 4\pi\sin\theta/\lambda$ with θ, half of scattering angle). The total scattering intensity is then

calculated with

$$I(\mathbf{Q}) = < Y(\mathbf{Q}, t) Y(-\mathbf{Q}, t) > = < Y(\mathbf{Q}, t) Y^*(\mathbf{Q}, t) >, \tag{3.2}$$

where <.......> means to take long time-average of quantity embodied in parentheses. The resolution of the scattering vector $\mathbf{Q}$ depends on the size of the crystal ($\mathbf{A}$, $\mathbf{B}$, $\mathbf{C}$). The small size of an MDS crystal may cause some extensions of diffraction spots.

3.2. Diffuse scattering

The calculations of scattering intensities at arbitrary $\mathbf{Q}$ are just straightforward, and applicable either to crystal or non-crystal. Here scattering at $\mathbf{Q}$ away from reciprocal lattice points is calculated for thermal vibrations in crystals.

Bragg scattering (0-th order scattering) is that occurring for atoms vibrating around their equilibrium positions without interacting themselves. It occurs when scattering vector $\mathbf{Q}/2\pi$ is superposed on reciprocal lattice vector $\mathbf{H}$ ($=h\mathbf{a}^*+k\mathbf{b}^*+\ell\mathbf{c}^*$). On the other hand, vibrating atoms in crystals interact each other, causing higher order scattering at non-zero wave vector $\mathbf{q}$. The number of wave vector $\mathbf{q}$, equal to the number of primitive unit-cells in crystal, is usually enormously large in real crystals, and therefore their distribution covers almost continuously the reciprocal space, the Brillouin zone (BZ). Since scattering intensities from a mode at wave vector $\mathbf{q}$ depends on its frequency and displacement pattern, its distribution in the BZ may provide useful information for dynamics of atoms in the crystal.

The total scattering appears as the addition of higher-order scattering to the 0-th order,

$$I(\mathbf{Q}) = I_0(\mathbf{Q}) + I_1(\mathbf{Q}) + I_2(\mathbf{Q}) + \ldots\ldots .$$

It may be practical to omit the second- and higher-order terms, since the higher-order terms are usually so small. The first-order intensity $I_1(\mathbf{Q})$ is contributed by the first-order scattering,

$$I_1(\mathbf{Q}) = \sum_{jq=1}^{nN} I_1(\mathbf{Q}, j\mathbf{q}),$$

where $I_1(\mathbf{Q}, j\mathbf{q})$ is calculated in the equation,

$$I_1(\mathbf{Q}, j\mathbf{q}) = \frac{(2\pi)^3}{V_{unit-cell}} \frac{E_{j\mathbf{q}}}{\omega_{j\mathbf{q}}^2} \sum_{\mathbf{H}} |F_1(\mathbf{Q}, j\mathbf{q})|^2 \ \delta_{\mathbf{Q}, \mathbf{q}+2\pi\mathbf{H}} . \tag{3.3}$$

$E_{j\mathbf{q}}$ and $\omega_{j\mathbf{q}}$ are the mean energy and the angular frequency, respectively, of mode $j\mathbf{q}$. $F_1(\mathbf{Q}, j\mathbf{q})$ is the first-order structure factor expressed in

$$F_l(\mathbf{Q}, j\mathbf{q}) = \sum_{\kappa}^{n} m_\kappa^{-1/2} f_\kappa(\mathbf{Q}) e^{-W_\kappa(\mathbf{Q})} [\mathbf{Q} \cdot \mathbf{e}_\kappa(j\mathbf{q})] e^{2\pi i \mathbf{H} \cdot \mathbf{r}_\kappa} \ , \tag{3.4}$$

where $\mathbf{r}_\kappa$ is the position vector of atom κ in the basic cell, averaged for time or lattice translations in the crystal, $e_\kappa(j\mathbf{q})$ the polarization vector of atom κ in mode $j\mathbf{q}$, m_κ the mass of atom κ. For deriving (3.4), we are indebted to Willis and Pryor (1975). It is possible to calculate each term in (3.3) and (3.4) for the MDS crystal, and therefore enable us to calculate the contribution from the first-order term separately. $E_{j\mathbf{q}}$, $\omega_{j\mathbf{q}}$ and $e_\kappa(j\mathbf{q})$ are calculated from the atomic trajectory data as described later in section 5. In such process, the modes causing the diffuse scattering could be identified.

4. Spectral analysis of MDS crystal

Power spectral densities are calculated with the FFT method applied to the trajectory data of MDS. The calculated spectra contain all the effects from thermal disturbances, and some of them are compared with the results of spectroscopic measurements such as Raman and IR. Some peaks in the spectral densities may be attributed to appropriate normal modes with the aid of lattice dynamical calculations or normal mode analysis of the trajectory data of MDS as described in section 5. Our chief concern is on the collective motions of atoms and their modes of vibrations. Spectra are calculated directly from FFT applied to the trajectory data. The FFT routines of Hino (1977) are employed in our package to calculate the power spectral density of MDS crystal.

4.1. Power spectrum

A random process $x(t)$, which is stationary and ergodic, is expressed by taking a standard Fourier integral for it sampled in time span $-T/2 \leq t \leq T/2$ as

$$x(t) \ = \int_{-\infty}^{\infty} |X(\omega)| e^{i(\omega t + \theta_\omega)} d\omega = \int_{-\infty}^{\infty} X(\omega) e^{i\omega t} d\omega \quad , \tag{4.1}$$

where θ_ω is the phase of constituent wave of frequency ω, and $x(t)$ is 0 outside the given time span $(-T/2, T/2)$. The Fourier transform of (4.1) is

$$X(\omega) = \frac{1}{2\pi} \int_{-T/2}^{T/2} x(t) e^{-i\omega t} dt \quad . \tag{4.2}$$

On the other hand autocorrelation function $C(\tau)$ is given as

$$C(\tau) = \lim_{T \to \infty} \int_{-T/2}^{T/2} x(t) x(t+\tau) dt . \tag{4.3}$$

Replacing $x(t)$ in (4.3) with (4.1) and reminding that $x(T)$ is 0 outside $(-T/2, T/2)$, the next expression is obtained,

$$C(\tau) = \int\limits_{-\infty}^{\infty} \left[\lim_{T \to \infty} \frac{2\pi X(\omega) X^{*(\omega)}}{T} \right] e^{i\omega\tau} d\omega, \tag{4.4}$$

where $X^*(\omega)$ is the complex conjugate of $X(\omega)$. When $\tau=0$, we obtain

$$C(0) \ = \ <x^2> \ = \ \int\limits_{-\infty}^{\infty} \left[\lim_{T \to \infty} \frac{2\pi X(\omega) X^{*(\omega)}}{T} \right] d\omega. \tag{4.5}$$

On the other hand, time average of x^2, $<x^2>$, is given using spectral density $S(\omega)$ as

$$<x^2> \ = \ \int\limits_{-\infty}^{\infty} S(\omega) d\omega. \tag{4.6}$$

Consequently the spectral density, i.e., mean energy per unit time is expressed as

$$S(\omega) = \lim_{T \to \infty} \left[\frac{2\pi \, | \, X(\omega) \, |^2}{T} \right] = \lim_{T \to \infty} \frac{1}{2\pi T} \left| \int\limits_{-T/2}^{T/2} x(t) e^{-i\omega t} dt \right|^2. \tag{4.7}$$

Returning to (4.4), we have two relations,

$$C(\tau) = \int\limits_{-\infty}^{\infty} S(\omega) e^{i\omega\tau} d\omega \tag{4.8}$$

and

$$S(\omega) = \int\limits_{-\infty}^{\infty} C(\tau) e^{-i\omega\tau} d\tau. \tag{4.9}$$

That is, power spectral density and correlation function is in a Fourier transform each other. We assume that the time-dependent systems in the following applications are stationary and ergodic random processes.

4.2. Power spectral densities of geometrical scattering amplitude

Now, we define our spectral densities. Atomic positions in crystals are time-dependent around their mean positions, and therefore $Y(\mathbf{Q}, t)$ in (3.1) is also time-dependent around the mean amplitude. Omitting time-independent terms from (3.1), we define the time-dependent geometrical scattering amplitude at wave vector $\mathbf{q}$ as

$$G(\mathbf{q},t) = \sum\limits_{\kappa}^{Z} e^{i\mathbf{q}\cdot\mathbf{r}_\kappa(t)}, \tag{4.10}$$

where $\mathbf{r}_\kappa(t)$ is the position vector of atom κ (1 to $Z=nN$) at time t. The Fourier transform of $G(\mathbf{q}, t)$ is

$$G(\mathbf{q},\omega) = \frac{1}{2\pi} \int\limits_{-T/2}^{T/2} G(\mathbf{q},t) e^{-i\omega t} dt,$$

and its spectral density is given in

$$S(q,\omega) = \lim_{T\to\infty} \frac{1}{2\pi T} \left| \int_{-T/2}^{T/2} G(q,t)e^{-i\omega t} dt \right|^2 .$$
(4.11)

In our calculation, the spectral density is first obtained from (4.11) applying FFT. If necessary, auto correlation function is calculated with (4.8). At $\mathbf{q} = 0$, $G(\mathbf{q}=0, t)$ contains no time-dependent term, and only an enormous peak appears at $\omega = 0$.

4.3. Power spectral density of atomic displacement parameter

The spectrum of atomic displacement parameter is expected to exaggerate that for specified atomic displacements. The normalized atomic displacement parameter as defined in (2.4) (Fig. 1) becomes the order parameter if averaged over time or space. Its spectral density must show that of QSM or TSM in the phase transition. Equation (2.4) is generalized to the case, where all the α_1 - α_2 joins are not in the single direction, but in unique-directions for site to site as

$$\delta_\kappa(t) = \frac{2u_{\kappa_{1-2}}(t)}{\Delta_{\kappa_{1-2}}},$$
(4.12)

where $u_{\kappa_{1-2}}(t)$ is the displacement of atom κ at time t from the high symmetry β-positions toward the low symmetry α_1 (or α_2). The normalizing constant $\Delta_{\kappa_{1-2}}$ is the α_1-α_2 separation at 0 K or its approximation. (The normalizing constant is not essential for spectrum, as noted before, but normalized $\delta_\kappa(t)$ is used for the order parameter.) The space Fourier transform of $\delta_\kappa(t)$ is defined in

$$\delta(\mathbf{q},t) = \sum_{\kappa=1}^{Z} \delta_\kappa(t)e^{i\mathbf{q}\cdot\mathbf{R}_\kappa} ,$$
(4.13)

where $\mathbf{R}_\kappa$ is the mean position vector of atom κ. The spectral density of $\delta(\mathbf{q}, t)$ is calculated with equation,

$$S(\mathbf{q},\omega) = \lim_{T\to\infty} \frac{1}{2\pi T} \left| \int_{-T/2}^{T/2} \delta(\mathbf{q},t)e^{-i\omega t} dt \right|^2 .$$
(4.14)

The normalized atomic displacement parameter in (4.12) is defined for the case of double-minimum potentials, but equation (4.12) could be applicable in more general cases, specifying displacement vectors; the normalizing constant is not serious, can be replaced by an arbitrary non-zero value, for the purpose of obtaining spectrum. This spectrum is free from the appearance of enormous 0-frequency peak when $\mathbf{q} = 0$, and superior for this point to other types of spectrum.

5. Normal mode analysis of MDS crystal

In the standard lattice dynamical calculation, the dynamical matrix is formed for the static

"averaged" structure concerned. The normal mode frequencies and polarization vectors are calculated from the *eigenvalues* and *eigenvectors*, respectively, of the dynamical matrix. In MDS, atom trajectories are available; their analysis may be more straightforward, in a sense, than preparing the dynamical matrix of static structure with assumed force parameters. Dove (1993) described the possible procedure for the normal mode analysis of the atom trajectories generated in MDS. However, the method has been not common so far for MDS crystal, and its reliability or usefulness has been not established. As already stated about the power spectral density of MDS crystal, the problem is how the spectra are assigned. We have attempted to apply the method to the trajectory data in MDS quartz.

An instantaneous displacement, $\mathbf{u}_{\kappa\ell}(t)$, of atom κ in the primitive cell ℓ from its equilibrium position is given as the sum of all contribution from $3nN$ normal modes,

$$\mathbf{u}_{\kappa\ell}(t) = (Nm_{\kappa})^{-1/2} \sum_{j\mathbf{q}} \left(\frac{E_{j\mathbf{q}}}{\omega_{j\mathbf{q}}^2} \right)^{\frac{1}{2}} \mathbf{e}_{\kappa}(j\mathbf{q}) \exp[i(\mathbf{q}\cdot\mathbf{r}_{\kappa\ell} - \omega_{j\mathbf{q}}t)], \qquad (5.1)$$

where $\mathbf{q}$ is the wave vector ($|\mathbf{q}| = 2\pi/\lambda$, λ is the wave length of mode $j\mathbf{q}$), m_{κ} mass of atom κ, $E_{j\mathbf{q}}$, and $\omega_{j\mathbf{q}}$ are average energy and angular frequency of mode $j\mathbf{q}$, respectively. The displacement in (5.1) is simplified using normal mode coordinate, $\Theta(\mathbf{q}, \omega_{j\mathbf{q}})$, as

$$\mathbf{u}_{\kappa\ell}(t) = (Nm_{\kappa})^{-1/2} \sum_{j\mathbf{q}} \mathbf{e}_{\kappa}(j\mathbf{q}) \Theta(\mathbf{q}, \omega_{j\mathbf{q}}) e^{i\mathbf{q}\cdot\mathbf{r}_{\kappa\ell}} . \qquad (5.2)$$

Polarization vector $e_{\kappa}(j\mathbf{q})$ represents the direction of displacement of atom κ in that mode, and orthonormalized as

$$\sum_{\alpha\kappa} e_{\alpha\kappa}^*(j\mathbf{q}) e_{\alpha\kappa}(j'\mathbf{q}) = \delta_{jj'} \qquad (\alpha = 1, 3).$$

Normal coordinate $\Theta(\mathbf{q}, \omega_{j\mathbf{q}})$ is just the mode $j\mathbf{q}$ vibrating with amplitude $(E_{j\mathbf{q}} / \omega_{j\mathbf{q}}^2)^{1/2}$ and with frequency $\omega_{j\mathbf{q}}$, and simply expressed as

$$\Theta(\mathbf{q}, \omega_{j\mathbf{q}}) = \left(\frac{E_{j\mathbf{q}}}{\omega_{j\mathbf{q}}^2} \right)^{1/2} e^{-i\omega_{j\mathbf{q}}t} . \qquad (5.3)$$

Let assume that the MDS crystal contains N primitive unit-cells, each contains n atoms. We define $3n$ space Fourier components of $\mathbf{u}_{\kappa\ell}(t)$ as

$$\mathbf{U}_{\kappa}(\mathbf{q}, t) = \left(\frac{m_{\kappa}}{N} \right)^{1/2} \sum_{\ell}^{N} \mathbf{u}_{\kappa\ell}(t) e^{-i\mathbf{q}\cdot\mathbf{r}_{\kappa\ell}} \qquad (5.4)$$

The preceding factor of the summation is to convert the displacement $\mathbf{u}_{\kappa\ell}(t)$ to the Fourier components for each atom. All terms in right hand side in (5.4) are available in MDS. It is noted that $\mathbf{U}_{\kappa}(\mathbf{q}, t)$ in (5.4) is expressed on the three components in the orthogonal coordinate system employed in MDS. Now let make a column matrix arranging the three components for an atom, and join them for all n atoms in a unit cell to make a big column

matrix $\mathbf{T}(\mathbf{q}, t)$ of $(3n \times 1)$ as

$$\mathbf{T}(\mathbf{q},t) = \begin{pmatrix} U_{11}(\mathbf{q},t) \\ U_{21}(\mathbf{q},t) \\ U_{31}(\mathbf{q},t) \\ U_{12}(\mathbf{q},t) \\ . \\ . \\ . \\ U_{3n}(\mathbf{q},t) \end{pmatrix}. \tag{5.5}$$

$\mathbf{T}(\mathbf{q}, t)$, expressed on the orthogonal coordinate of the MDS crystal, is transformed to that of normal coordinates as shown below.

First, a $(3n \times 3n)$ Hermite matrix is prepared taking transposed matrix of complex conjugate of $\mathbf{T}(\mathbf{q}, t)$, $\widetilde{\mathbf{T}}(\mathbf{q}, t)^*$ as

$$\boldsymbol{\Psi}(\mathbf{q},t) = \mathbf{T}(\mathbf{q},t)\,\widetilde{\mathbf{T}}(\mathbf{q},t)^*. \tag{5.6}$$

Assuming that $\mathbf{T}(\mathbf{q}, t)$ is transformed to time-dependent normal mode vector $\boldsymbol{\Theta}(\mathbf{q}, t)$ with a transformation matrix $\mathbf{A}(\mathbf{q})$, i.e.,

$$\boldsymbol{\Theta}(\mathbf{q}, t) = \mathbf{A}(\mathbf{q})\mathbf{T}(\mathbf{q}, t). \tag{5.7}$$

The time-average of column vector $\boldsymbol{\Theta}(\mathbf{q}, t)$ and its transposed conjugate complex vector $\widetilde{\boldsymbol{\Theta}}(\mathbf{q}, t)^* \; (= \widetilde{\mathbf{T}}(\mathbf{q}, t)^* \, \widetilde{\mathbf{A}}(\mathbf{q})^*)$ is given as

$$<\boldsymbol{\Theta}(\mathbf{q},t)\,\widetilde{\boldsymbol{\Theta}}(\mathbf{q},t)^*> = \mathbf{A}(\mathbf{q}) <\mathbf{T}(\mathbf{q},t)\,\widetilde{\mathbf{T}}(\mathbf{q},t)^*> \widetilde{\mathbf{A}}(\mathbf{q})^*$$
$$= \mathbf{A}(\mathbf{q}) <\boldsymbol{\Psi}(\mathbf{q},t)> \widetilde{\mathbf{A}}(\mathbf{q})^* \tag{5.8}$$

Since the normal mode coordinates are orthogonal each other, the left side of (5.8) must be diagonalized. That is, the right side of (5.8) is the process for diagonalizing matrix $<\boldsymbol{\Psi}(\mathbf{q}, t)>$. Each of $3n$ elements of left side of (5.8) may correspond to the normal coordinates $<\boldsymbol{\Theta}(\mathbf{q}, \omega_{j\mathbf{q}})>$, and we can relate the frequency and the average energy of mode with

$$|\boldsymbol{\Theta}(\mathbf{q},\omega_{j\mathbf{q}})|^2 = \boldsymbol{\Theta}^*(\mathbf{q},\omega_{j\mathbf{q}})\boldsymbol{\Theta}(\mathbf{q},\omega_{j\mathbf{q}}) = \frac{E_{j\mathbf{q}}}{\omega_{j\mathbf{q}}^2}. \tag{5.9}$$

Since the diagonal elements of the diagonalized matrix on the left side of (5.8) is the eigenvalues of $<\boldsymbol{\Psi}(\mathbf{q}, t)>$, it is not necessary to find the transformation matrix $\mathbf{A}(\mathbf{q})$, because $3n$ eigenvalues are directly determined applying standard routine such as

Householder method to $\langle\Psi(\mathbf{q}, t)\rangle$. Putting the eigenvalue as δ_{jq}^2, the harmonic frequency ω_{jq} is calculated as

$$\omega_{j\mathbf{q}}^2 = \frac{E_{j\mathbf{q}}}{\delta_{jq}^2} \tag{5.10}$$

and $3n$ polarization vectors of mode $j\mathbf{q}$ are given with $3n$ eigenvectors. For reference, transformation matrix $\mathbf{A(q)}$ is given by arranging $(3n\times1)$ eigenvectors $\mathbf{V}_{jq}|$ for j-th eigenvalue in the square matrix such as

$$\mathbf{A(q)}=(\mathbf{V}_1| \; \mathbf{V}_2|......\mathbf{V}_j|.....\mathbf{V}_{3n}|). \tag{5.11}$$

In our computer program, total energy E_{jq} is evaluated taking the high temperature approximation, i.e., equal partition of energy over mode, and the diagonalization of $\langle\Psi(\mathbf{q}, t)\rangle$ is done without symmetry restraints. In application to MDS quartz, some obviously inconvenient results occurred in polarization vectors. We consult with group theoretical analysis to overcome this problem.

6. Examples of application to MDS quartz
6.1. Brief review for the structure of quartz and its change

The structure of quartz is constituted of a framework of SiO_4 units, which are linked to neighbor units by sharing all the corner O atoms. The space group is either $P3_221$ or $P3_121$ for α-quartz, which is known to transform to the hexagonal polymorph with space group $P6_222$ or $P6_422$, respectively, at around 846 K. The atom positions in a α-phase crystal of single domain at low temperatures such as room temperature are usually referred as "α_1-positions" (Young, 1962). There is another set of positions, "α_2-positions". The position corresponding to the middle of α_1 and α_2 positions are sometime called as "β-position". The SiO_4 units are believed rather rigid, and the atom positions are usually expressed with the orientations of the units, such as "atoms in α_1-orientations or in α_2-orientations". The two orientations or sets of positions are related by the rotational operation of corner-linked SiO_4 units around the $<100>$ axes (2-fold axes) passing the central Si atoms, being associated by the small translational operation along the axes. That is, the α_1 and α_2 orientations are related by the screw operation of corner-linked SiO_4 via the corresponding β-orientations. The angle is calculated rather great as about $30°$ at room temperature, but the atomic separations are not so; about 0.8 Å at the O-site and 0.34 Å at the Si site (Young, 1962; Kihara, 1990). On the other hand, in the diffraction studies, the atomic positions for Si and O atoms in hexagonal β-quartz are assigned either to the corresponding β-positions (single-minimum model) or to both the α_1 and α_2 site with equal weight (50-to-50) (double-minimum model or split-site model). These different views of β-quartz are directly related to the different interpretations for the α-β polymorphic transition. One is represented by Young (1962): the atom equilibrium positions continuously change from

those in the α-phase, say the α_1-positions, to those at the β-positions with increasing temperature. This may imply that the minima of potentials at atom sites continuously shift toward the corresponding β-positions with increasing temperature in α-quartz, and finally reach the β-positions of single-minimum in the β-phase. Another is based on the idea of domains in the α_1 and α_2 orientations (for example, Wright and Lehmann, 1981). In the domain idea, the structure of quarts is the average of the domains in the two orientations: the ratio of α_1 and α_2 domains varies with temperature in the α-phase, but kept equal in the β-phase. The domains may possibly be dynamic, changing time to time, or place to place.

Four A_1 normal modes can occur theoretically at Γ in α-quartz, see (7.1), but it is reported that an extra band appears in Raman measurements (Shapiro et. al., 1967; Scott, 1968). Figure 2 of Shapiro et. al. (1967) shows the temperature dependence of A_1 Raman bands of quartz. A small 147 cm^{-1} band at 306 K, considered as the extra band (satellite band), grows, but softens quickly with increasing temperature. The 206 cm^{-1} band, believed as the soft mode of the α-β transition (for example, Ercombe, 1967), shows rather weak softening, and appears not frozen at the transition point.

The methods shown in sections 3, 4 and 5 were applied to analyze the collective motions of atoms in MDS quartz in expecting to draw a determinative conclusion for the mechanism of the structural changes in quartz, together with the associated phenomena such as the strange thermal expansion behaviors, the A_1 satellite band, characteristic diffuse scattering and so on. Here some selected results are described, focusing mainly on the atom displacement parameter, power spectral densities and normal mode analysis. It was confirmed that the α- and β-phases of MDS quartz belong to space groups $P3_221$ and $P6_222$, respectively. (Our MDS was started with α-quartz in $P3_221$.)

6.2. Time dependent atomic displacement parameter and order parameter

Time dependent atomic displacements calculated with equation (2.4) for selected atoms in our MDS quartz (Kihara 2001 a) suggest for TSM to be exited at some low temperatures below the transition point, likely for the model structure in 2.4.1. The order parameter was calculated for the displacements of atoms from the β-positions taking the $\alpha_1-\alpha_2$ components. The normalizing constant $\Delta_{\kappa_{1-2}}$ of (4.12) was approximated to the corresponding separations between the α_1 and α_2 positions at 300 K. This one-dimensional order parameter η is thus unity at 300 K, and expected to remain nearly unity below this temperature. The order parameters calculated with (2.6) for each atom in the unit-cell and calculated with (2.5) for the unique η representing the crystal are all almost equal each other, suggesting that the structural change is driven by the displacements of atoms at all the sites activated by QSM and/or TSM.

Fig. 2 shows the temperature evolution of η calculated with (2.5). It is well known that the temperature evolution of thermodynamic function in the α-β transition in quartz is first-order in a rigorous sense, but appears as second-order-like. A thermodynamic function
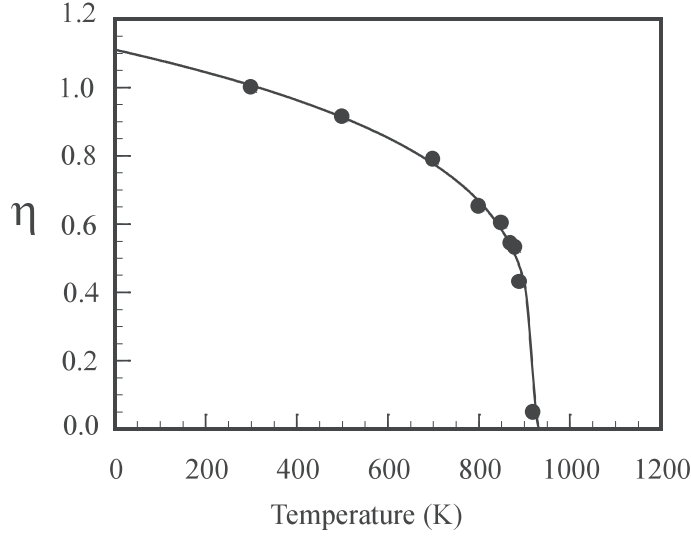
Fig. 2. Temperature dependence of order parameter for quartz in a molecular dynamics simulation. Solid circles represent values for molecular dynamics simulation, which are fitted as the curve of solid line with equation (6.2) in text.

in the first-order change may be well approximated by the Landau expansion including the terms up to the 6-th order,

$$\Phi(p,T,\eta) = \Phi_o(p_c,T) + a(T - T_o)\eta^2 + b\eta^4 + c\eta^6..., \tag{6.1}$$

where the parameters a, b and c are restrained as $b<0$, a, $c>0$ to guarantee the transition to be the first-order, and T_o is a temperature lower than the critical temperature T_c. The order parameter η is 0 in the β-phase, but changes with temperature in the α-phase as

$$\eta(T) = \pm\left(\frac{2}{3}\right)^{1/2}\eta(T_c)\left[1 + \sqrt{1 - \frac{3(T - T_o)}{4(T_c - T_o)}}\right]^{1/2}. \tag{6.2}$$

The conditions for the minimum and maximum of thermodynamic function Φ guarantee five real roots, if temperature T satisfies a condition $T_o \leq T \leq T_o + b^2/3ac$. At T_c, Φ contacts with the η axis ($\Phi=0$) at $\eta=0$ and $\pm\eta$. In Fig. 2, η is plotted for all the points of MDS quartz in the range from 300 to 1400 K. Fitting the data points between 300 and 900 K with (6.2) provides $T_c \approx T_o \approx 920$ K, and $\eta(T_c) = 0.02$. These values suggest that this transition is nearly the second-order, or otherwise the fourth-order term in (6.1) disappears. The result is in a weak contrast to the value of T_c - T_o ($\approx 7°$K) for real quartz (Kihara, 2001 c). We consider that our MDS quartz is so small, and our values represent for that small quartz with given energy parameters.

The behavior of the time-dependent atomic displacement parameter, normalized as (4.12), suggests that TSM as shown in the model structure composed of atom sites with

double-minimum potentials is already excited at some low temperatures (around 600 K) below the transition point in MDS quartz. So in MDS quartz, there may be two A_1 modes corresponding to QSM for small amplitude motions confined in the wells and TSM for large amplitude oscillations over the two corresponding wells.

6.3. Power spectral density

Fig. 3 illustrates the power spectral densities along Γ-M for the geometrical scattering amplitudes in (4.10) for the MDS at 300 K. (M is the points on the zone boundaries perpendicular to $\mathbf{a}^*$ and its symmetry equivalent directions.) The case for $\mathbf{q} = 0$ is not shown, because it has no oscillatory component. There are 27 peaks expected at $\mathbf{q}=[0\ \xi\ 0]$, i.e., along Γ-M, for both the phases of quartz. We can see about 20 peaks in Fig. 3, showing some characteristic features of distribution: the first is that all the peaks appear below 40 THz, the second that three to four peaks appear between 30 and 40 THz, which are known to the spectra for the deformation of SiO_4, the third that no peak is seen in 25 - 30 THz, the fourth that the dispersion is small for peaks above 10 THz, which may be characteristic for the optic modes, and the fifth that the dispersion relations for the spectra below 10 THz are complicated, probably due to the acoustic branches. These features are all quite in good harmony with the observed ones for quartz, that is, our MDS quartz successfully represents the frequency distribution of phonon spectrum of quartz.

The power spectral density was then calculated for the components of atomic displacements in the α_1 - α_2 lines $u_{x_{1-2}}(t)$ in (4.12). Fig. 4 illustrates the temperature
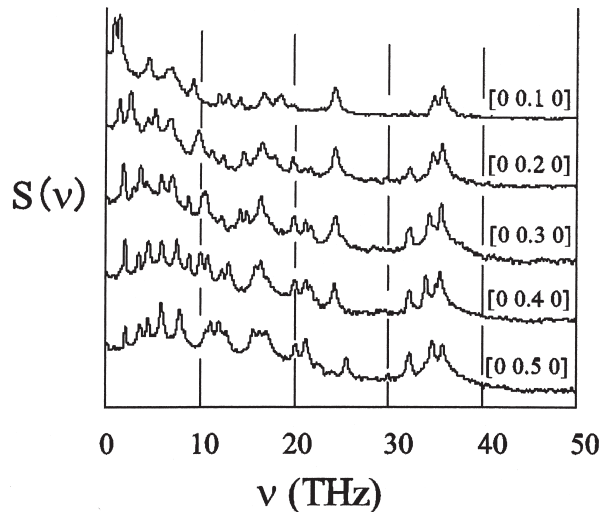
Fig. 3. Power spectral densities $S(\nu)$ (sec) in an arbitrary logarithmic scale along Γ-M calculated with atomic trajectories in a molecular dynamics simulation of quartz at 300 K. Wave vectors are indicated with the aid of hexagonal reciprocal lattice vectors such as [0 0.1 0] for $\mathbf{q} = 0.1\ \mathbf{b}^*$ and so on.
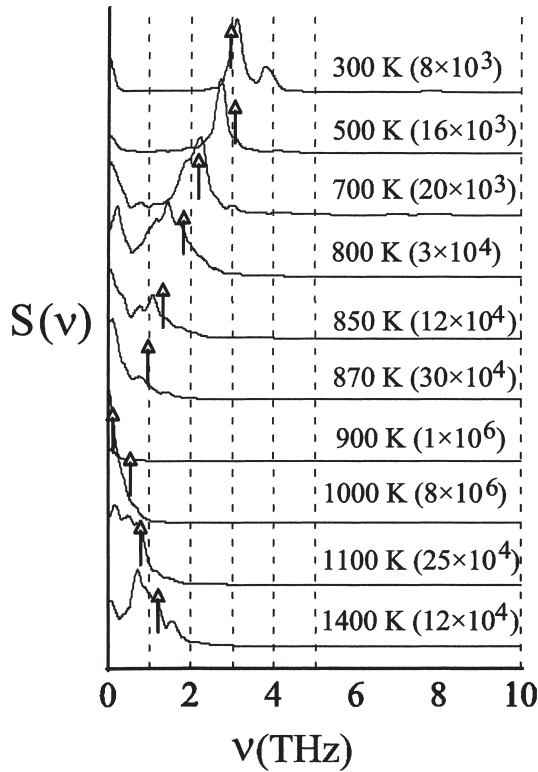
Fig. 4. Temperature evolution of power spectral densities of time-dependent atomic displacement parameter at $\Gamma(\mathbf{q} = 0)$. Spectra below 10 THz are indicated in arbitrary linear scales, whose maximum values are indicated in parentheses following temperature values.

dependence of the spectra below 10 THz, obtained for $\delta(\mathbf{q}=0, t)$ with (4.13). The spectrum in the higher frequency zone appears to share most common features with that observed for geometrical scattering amplitudes. Through all the temperatures studied, a peak of low frequency is predominant, as expected. That band appeared at about 3 THz at 300 K quickly shifts toward the low frequency side with increasing temperature; it becomes a huge peak nearly at $\nu = 0$ at 900 K, and begins to shift toward the higher frequency side with further increase of temperature. The temperature dependence of this band is well comparable with the A_1-satellite band at 147 cm^{-1} (4.41 THz) observed in the Raman experiments of α-quartz at room temperature (Figure 2 of Shapiro et al., 1967). Later in the normal mode analysis, this band is assigned to QSM or/and TSM, which drives the α-β transition in quartz.

6.4. Normal mode analysis
6.4.1. Evaluation of performance
The normal modes in MDS quartz were analyzed assuming the ordered structure, that is,

27 normal modes occur at each wave vector **q**. In the analysis of MDS quartz, the transfer mode (TSM) excited as an extra mode, may cause a difficulty in assignment. If TSM belongs to the same symmetry as the A_1 normal mode (QSM), and both are excited, the present analysis would result in an erroneous frequency (probably the averaged value for both). Irrespective of this expected difficulty, the normal mode analysis was performed taking the part of 82 ps from a long time-series. The frequencies and the atomic displacement patterns of modes were compared with the corresponding observations for quartz to examine the present performance.

Figs. 5 a, b, c illustrate the displacement patterns of atoms in MDS quartz, which are the exaggerated polarization vectors in the QSM or/and TSM at **q** = 0: a. 300 K, b. 895 K, c. 1200 K. Since TSM is not to be excited at 300 K, the pattern at 300 K may be of QSM. However, the patterns at 895 and 1200 K must be dominated by TSM or its successor mode in the β-phase. The displacement patterns for the β-phase (Fig. 5 c) comply with the
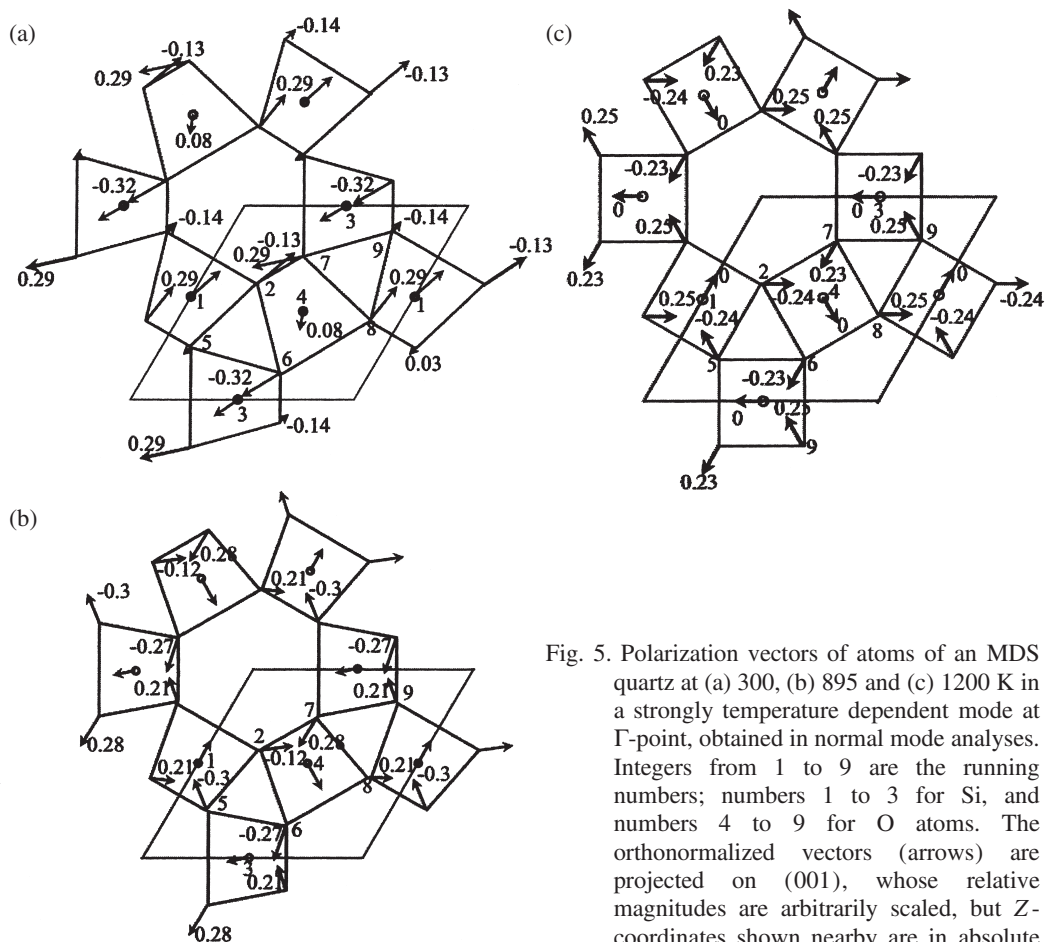
Fig. 5. Polarization vectors of atoms of an MDS quartz at (a) 300, (b) 895 and (c) 1200 K in a strongly temperature dependent mode at Γ-point, obtained in normal mode analyses. Integers from 1 to 9 are the running numbers; numbers 1 to 3 for Si, and numbers 4 to 9 for O atoms. The orthonormalized vectors (arrows) are projected on (001), whose relative magnitudes are arbitrarily scaled, but Z-coordinates shown nearby are in absolute values.

Table 1. Character tables for point groups of quartz

a. At Γ-point of low quartz

32 (D_3)	I	$2\,C_{3[001]}$	$3\,C_{2[100]}$
A_1	1	1	1
A_2	1	1	−1
E	2	−1	0

b. At Γ-point of high quartz

622(D_6)	I	$2\,C_{6[001]}$	$2\,C_{3[001]}$	$C_{2[001]}$	$3\,C_{2[120]}$	$3\,C_{2[100]}$
A_1	1	1	1	1	1	1
A_2	1	1	1	1	−1	−1
E_1	2	1	−1	−2	0	0
E_2	2	−1	−1	2	0	0
B_1	1	−1	1	−1	1	−1
B_2	1	−1	1	−1	−1	1

c. In Γ-M of high quartz

2(C_2)	E	$C_{2[120]}$
$\Sigma_1(A)$	1	1
$\Sigma_2(B)$	1	−1

d. At M-point in high quartz

222(D_2)	I	$C_{2[001]}$	$C_{2[100]}$	$C_{2[120]}$
$M_1(A)$	1	1	1	1
$M_2(B_1)$	1	1	−1	−1
$M_3(B_3)$	1	−1	1	−1
$M_4(B_2)$	1	−1	−1	1

B_1 representation (Tab. 1), well known for the soft mode in β-quartz. It is also seen for α-MDS quartz that the displacement pattern nearly satisfies the A_1 symmetry at high temperatures (Fig. 5 b), but not well at low temperatures (Fig. 5 a). Beside these inconsistencies, the obtained frequencies appear comparable with those estimated from the peak positions in the power spectrum density.(In Fig. 4, the frequencies of QSM or/and TSM in the present normal mode analysis are indicated with arrows.)

As stated, the performance of the normal mode analysis of MDS quartz appears different at low temperatures and at high temperatures. It has not been answered so far

what cause the difference. Since our main concern is on the low frequency modes at high temperatures near the phase transition, the normal mode analysis is performed mainly for the low frequency modes.

6.4.2. Low frequency Γ-*M* branches

Fig. 6 illustrates the dispersion relations of low frequency Γ-*M* branches, an optic and three acoustic branches, of the β-phase of MDS quartz at 1400 K: #1 and 2 are the transversal acoustic branches in antisymmetric Σ_2 (Table 1), #3 the longitudinal acoustic one in totally symmetric Σ_1, and #4 the optic branch in Σ_2. The dispersion relations and their temperature dependences for our MDS quartz are well comparable and rather in good agreement with those for inelastic neutron scattering measurements by Dolino et al. (1992). The characteristic features in these low-frequency Γ-M branches obtained in the normal mode analysis of MDS quartz are briefly viewed below taking the case of β-phase, with the aid of Fig. 7 illustrating the displacement patterns in the zone boundary *M*-point modes of the #1 and 2 branches at two temperatures just below and above the transition point.

The #4 optic branch (Σ_2) is connected to the SM (B_1) at Γ. The #1 branch is dominated by transversal acoustic strains in $\Sigma_2(B)$ with dominant component in X (denoted as TA_X), containing some amounts of the SM (B_1) components. The #2 branch shows the clear TA_Z character in Σ_2 at small **q** from 0 to about 0.2 **b***, but that character disappears at **q** larger
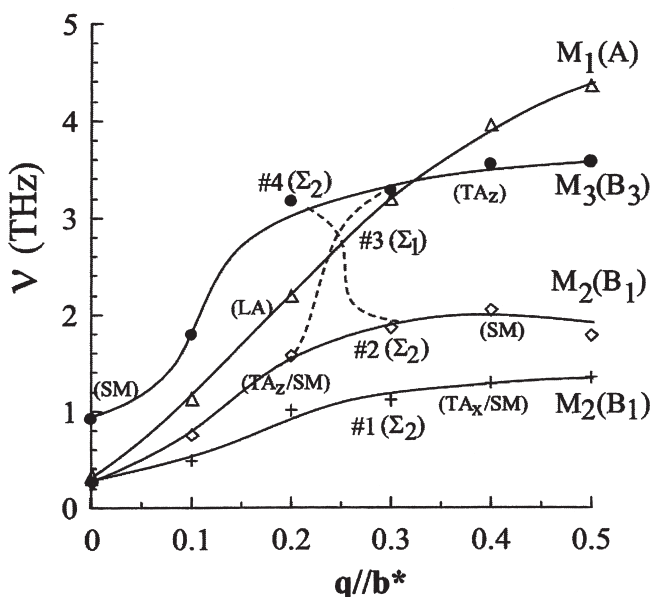
Fig. 6. Dispersion relations in four low-lying branches of MDS quartz in Γ-*M* at 1400 K. The branches are numbered in the sequence from the lowest to the higher branches. M_1 to M_3 are the symmetry representations at zone boundary *M*-points, and Σ_1 and Σ_2 at Γ-*M*. See Table 1. The eigenvectors are exchanged between #2 and #4 branches in the range 0.2 ~ 0.3 **b***.

Fig. 7. Atomic displacement patterns at zone-boundary *M*-point deduced from harmonic lattice dynamical approaches to MDS quartz. The orthonormalized vectors (arrows) are projected on (001), whose relative magnitudes are arbitrarily scaled, but the *Z*-coordinates shown nearby are in absolute values.
 (a) Branch #1 at 975 K, (b) Branch #2 at 975 K, (c) Branch #1 at 1400 K, and (d) Branch #2 at 1400 K.

than 0.3 **b***. On the other hand, the #4 branch in Σ_2 loses the SM character at **q** from 0.2 to 0.3 **b***, but then gains the TA_Z characters to the *M*-point. These unexpected changes in branches #2 and #4 appear correlated each other, suggesting the exchange of the eigenvectors between them. The optic SM and TA_1 in quartz are considered to couple

strongly with each other via strain and its space gradient (Aslanyan and Levanyuk, 1979). In the present MDS quartz, branch #4 can couple not only with #1 (TA_X), but also with #2 (TA_Z), both in the same symmetry. Taking the suggested eigenvector exchange between #2 and #4 into consideration, it may be reasonable to conclude that, at **q** smaller than about 0.2 **b***, the softening of the SM (#4) at **q** near 0 causes #2 (TA_Z) to be softened, and also #1 (TA_X) via the mode coupling. The #3 acoustic branch is free from such coupling with other modes, and keeps the longitudinal character (LA) in Σ_1

The exchange or mixing of the polarization vectors between the #2 (TA_Z) branch and the optic soft branch in Γ-M are also observed at high temperatures in the α-phase of MDS quartz. Such exchange does not occur at 300 K. We consider that the eigenvector exchange is associated by the excitation of the large-amplitude transfer modes, i.e., A_1 TSM (optic mode) in the α-phase and B_1 SM in the β-phase. The #4 optic branch strongly softens at Γ with temperature approaching to the transition point from below, causing the two acoustic branches #1 and #2 to soften via mode coupling at small **q** around 0.1 **b***. These low frequency branches are shown to cause the diffuse scattering observed in diffraction experiments (Kihara and Matsui, 2003). If the MDS crystal were large enough, the branches could give incommensurate satellite reflections on **a*** (**b***) near the α-β transition point.

7. β-phase structure and α-β transition in quartz
7.1. Structure of β-quartz

There have been a number of discussions about the β-phase structure of quartz since Young (1962), who preferred the single-minimum model of potentials in the X-ray diffraction study of the β-phase. On the contrary, Wright and Lehmann (1981) succeeded to refine an α_1–α_2 split-atom model with neutron diffraction data, leading them to prefer the α_1-α_2 domain model. We consider that the successful refinement of the latter authors is not essential to support the superiority of the split-atom model to the single-minimum model. Actually Kihara (1990) succeeded to refine the single-minimum model assuming generalized structure factors in a better agreement factor between observed and calculated structure amplitudes than the split-atom model. For example, Kihara (1990) obtained extended, but unimodal probability density functions (pdf) either site for O or Si. The atom pdfs in our MDS quartz were all unimodal both in the α and β phases (Kihara, 2001 a). On the other hand, the time-series of $\delta_\kappa(t)$ and its temperature dependence for arbitrarily chosen atom sites show the double-minimum characteristic (Kihara, 2001 a). Both the results obtained with our MDS quartz prove that the unimodal pdfs in the β-phase are resulted from the double-minimum potentials. The success of the split-atom refinement only shows that the pdf in quartz is not so simple as expressed by a normal Gaussian distribution. If atoms can move almost freely over the energy barriers of double-minimum potentials, the pdfs obtained in usual diffraction experiments could be extended, but unimodal, depending on the form of potential energies.

7.2. Soft mode in quartz

The point groups of α- and β-quartz are 32 and 622, respectively. The 27 modes at Γ are assigned as

$\Gamma = 4\,A_1(\text{R}) + 4\,A_2(\text{IR}) + 8\,E\,(\text{R,IR}) + 1\,A_2(\text{A}) + 1\,E\,(\text{A})$ for α-quartz, and

$\Gamma = 1\,A_1(\text{R}) + 2\,A_2(\text{IR}) + 3\,B_1 + 2\,B_2 + 4\,E_1(\text{R,IR}) + 4\,E_2(\text{R}) + 1\,A_2(\text{A}) + 1\,E_1(\text{A})$ for β-quartz,   (7.1)

where Raman and IR active representations are denoted with R and IR in parentheses, respectively, and acoustic modes are with A in parentheses. In (7.1), B_1 and B_2 modes are silent mode. Shapiro et al. (1967) found an extra A_1 band of 147 cm^{-1} (4.4 THz at room temperature) in a Raman measurement of α-quartz. In usual lattice dynamical calculations of α-quartz at room temperature, the band of 207 cm^{-1} (6.21 THz) is assigned as the soft mode of A_1 symmetry (For example, Elcombe, 1967). However, the frequency of the A_1 band shows only weak temperature dependence with no sign of freezing out at the transition point and even in β-quartz. The band strongly softens is the satellite band of 147 cm^{-1}. Scott (1968, 1974) explained the possibility of the satellite band and its temperature evolution with Fermi resonance. We stressed here another possibility such that the strongly temperature dependent band, i.e., the transfer mode TSM observed in MDS quartz corresponds to the satellite mode observed in the Raman measurement.

TSM and QSM may possibly be mixed up as a single mode in the normal mode analysis. Because TSM is not excited at 300 K in our MDS quartz, the dominant peak observed at 3 THz in the power spectral density (Fig. 4) may correspond to QSM. On the other hand, the behaviors seen in the atomic displacement parameters (Kihara, 2001 a) suggest that TSM is excited at some higher temperature, probably already excited at 600 K. The widening of the peak at 700 K (Fig. 4) is probably due to the partial superposition of QSM and TSM. The amplitude of TSM is expected greater than that of QSM, and therefore the frequency of TSM is expected lower than that of QSM. TSM rapidly softens to the huge peak of $\nu \approx 0$ at 900 K, the transition point in our MDS quartz. On the other hand, QSM is only weakly softened with increasing temperature. There is no peak corresponding to QSM observed at 900 K and 1000 K (Fig. 4 in linear scale): this may arise from the decrease of relative intensity of QSM compared to TSM.

Now consider the temperature dependence of the frequency of TSM, ν_{TSM} ($\mathbf{q}$=0), in the α-phase of MDS quartz. Taking the observed temperature dependence of ν_{TSM}, which softens to 0 when temperature approaches to T_c, we assume that ν_{TSM}^2 ($\mathbf{q}$=0) is proportional to $(\Delta E - k_B T)^{\alpha}$, where ΔE is the barrier height for the mode (probably equivalent with the average of heights at all the sites), and k_B is the Boltzmann constant. Putting ΔE as $k_B T_c$, we obtain a relation containing the order parameter η,

$$\nu_{\text{TSM}}^2(\mathbf{q}=0) \propto (T_c - T)^{\alpha} = c \times \eta^{\alpha/\beta}.$$ (7.2)

We obtain 6.5 for α/β in fitting with (7.2). By analogy with a simple lattice dynamics, ν_{TSM}^2 is expected to be proportional with the restoring force associated with the mode, suggesting that the restoring force is proportional to η to about 6-th power. This may suggest that the potentials extend with only weak slopes in the vicinity of $\eta = 0$.(Let remind that η varies between 0~1.)This is another evidence to show that the atoms in MDS quartz can move almost freely over the energy barriers at high temperatures to result to the unimodal atomic distributions.

7.3. Structural changes in quartz

The atomic motions in MDS quartz are summarized here. At low temperatures (below 600 K), our MDS quartz is perfectly ordered with atoms undergoing thermal vibrations confined in, say, the α_1-wells of potentials. In the A_1 Γ-point normal mode (denoted as QSM) with frequency about 3 THz, atoms oscillate around the α_1-minima, being confined in the α_1-wells; the motions of atoms can be collected as the screw oscillations of SiO_4 units around <100>. With increase of temperature, some atoms are energized to move over the energy barriers (β-positions) to the α_2-wells. The transfer α_1->α_2 or α_2->α_1 occurs equally at every site. This is confirmed by knowing that η obtained with (2. 6) is equal for each atom. This is the result of collective motions of atoms, and shows that a vibrational mode, denoted as TSM, other than the normal modes is excited as an extra mode. This mode also belongs to the A_1 rep, and is driven by QSM of frequency about 3 THz, via strong coupling through the structural deformations with the same symmetry. The frequency of TSM can vary from 0 to the maximum of that of the A_1 QSM. With increasing temperature, QSM changes to less significant, while TSM becomes remarkable. At the temperature, where both the wells α_1 and α_2 are occupied equally by atoms, the restoring force of TSM becomes null, and the α-β transition is completed. With further increase of temperature, the mode average energy (k_BT in the high temperature approximation) rises, and therefore the effective mean potentials become to of single-minimum-like, and the transfer mode becomes to be identified as the B_1 normal mode. Inversely when the mode energy approaches the level of the barrier from above, the effects of the double-minimum appear in the atomic motions, i.e., the $\alpha_1 \leftrightarrow \alpha_2$ restoring force is recovered, and instead of the B_1 mode, the A_1 TSM appears.

8. Computer programs

Our MDS is calculated with computer program CTPMD (Matsui, 1988), partially modified for the parts writing out the results for the analysis. In our CTPMD, the time-series of all the atoms are stored in sequential-unformatted file "save 9.dat", and the necessary data for further calculations of simulations are saved in formatted "save 4.dat". The program package MDPROC contains four programs, listed below, all written in FORTRAN.

(1) MDSTR

　　Calculate the quantities ready to compare with those of usual structure analyses.

　　Atomic fractional coordinates and size of MDS crystal, both in time and ensemble averaged

　　Atomic mean square displacements and probability density functions in contours

　　Atomic distances and angles in time and ensemble averages

(2) MDOPSPECT

　　Order parameters (macroscopic)

　　Power spectrum densities for atomic displacement parameters

(3) MDNORMODE

　　Frequencies and polarization vectors of normal modes

(4) MDSPECT

　　X-ray scattering intensities

　　X-ray diffuse scattering

　　Power spectrum densities for geometrical scattering amplitudes

9. Summary

In this article, the procedures for analyzing time-series data of atoms generated in molecular dynamics simulation were described for the calculations of bond distances and angles, mean square displacements and probability density functions of atoms, power spectral densities and normal mode analysis. The methods were applied to the atom trajectories in MDS quartz to discuss the dynamic nature of atoms in quartz, which have remained controversial for long time.

　　The power spectral densities of space Fourier components of time-dependent atomic displacement parameters calculated for the α_1-α_2 directions at atom sites showed a single dominant band behaving like the soft mode of the α-β transition. The polarization vectors and frequencies of the 27 possible normal modes for quartz were calculated at different values of $\mathbf{q}$. At high temperatures, the dispersion curves of low frequency branches were well comparable with the measured ones in experiments (inelastic neutron scattering) particularly in the β-phase region. These results were used to discuss the causes of the strong softening near the transition point occurring in the low frequency branches in Γ-M. The two lowest frequency acoustic branches containing transversal characters and an optic branch share the same symmetry and therefore can couple themselves, and also eigenvector exchange occurs between the optic mode and the second lowest acoustic branch at $\mathbf{q}$ in range 0.2 to 0.3 $\mathbf{b}$*. The present analysis also showed that the temperature dependences of the three low frequency branches (two transversal acoustic and one optic branches) are essentially important to generate the incommensurate satellite reflections on $\mathbf{a}$* ($\mathbf{b}$*) via coupling.

　　The model based on double-minimum potentials at atom sites proposed with the present results of analysis of MDS quartz is also successful to explain the thermal

expansion behaviors of Si-O bond distances and cell dimensions. The subject appears somewhere else (Kihara, 2001 b), and was not discussed here.

References

Dolino G., B. Berge. M. Vallade. F. Moussa (1992) Origin of the incommensurate phase of quartz: I. Inelastic neutron scattering study of the high temperature β phase of quartz. J. Phys. I France 2, 1461-1480.

Dove M T. (1993) Introduction to lattice dynamics. In Cambridge topics in mineral physics and chemistry. Cambridge University Press

Elcombe M. M. (1967) Some aspects of the lattice dynamics of quartz. Proc. Phys. Soc. 91, 947-958.

Hino M. (1977) Spectral analysis (in Japanese). Asakura, Tokyo

Kihara K. (1990) An X-ray study of the temperature dependence of the quartz structure. Eur. J. Minerals. 2, 63-77.

Kihara K. (2001 a) Molecular dynamics interpretation of structural changes in quartz. Phys. Chem. Minerals. 28, 365-376

Kihara K. (2001 b) Thermal expansions in quartz: A geometrical consideration. Journal of Mineralogical and petrological Sciences, 96, 159-163.

Kihara K. (2001 c) Crystal structures of silica polymorphs and their phase transitions (in Japanese). Journal of Crystallographic Society of Japan, 43, 218-226.

Kihara K. and N. Matsui (2003) Molecular dynamics study and normal mode analysis of diffuse scattering in quartz. Phys. Chem. Minerals. 30, 345-352

Matsui M. (1988) Molecular dynamics study of $MgSiO_3$ perovskite. Phys. Chem. Mineral 16, 234-238.

Scot J. F. (1968) Evidence of coupling between one and two phonon excitations n quartz. Phys. Rev. Letters, 21, 907-910.

Scot J. F. (1974) Soft mode spectroscopy : experimental studies of structural phase transitions. Rev. Mod. Phys., 46, 83-128.

Shapiro, S M, D. C. O'Shea, H. Z. Cummins (1967) Raman scattering study of the α-β transition in quartz. Phys. Rev. Letters 19, 361-364

Willis B.T.M. and A. W. Pryor (1975). Thermal vibrations in crystallography. Cambridge University Press, pp. 1-280.

Wright, A. F. and S. Lehmann (1981) The structure of quartz at 25 and 590°C determined by neutron diffraction. J. Solid State Chem., 36, 371-380.

Young, R. A. (1962) Mechanism of the phase transition in quartz. Report 2569, Air Force Office Scientific Research, Washington 25, D.C.